THE PHOTOCHEMISTRY AND DYNAMICS OF A DUSTY COMETARY ATMOSPHERE

M. L. MARCONI* and D. A. MENDIS†

Center for Astrophysics and Space Science, University of California, San Diego, La Jolla, Cal., U.S.A.

(Received 19 May, 1982)

Abstract. A self-consistent solution of the dynamical and thermal structure of an H_2O-dominated, two-phase, dusty-gas cometary atmosphere has been obtained by solving the simultaneous set of differential equations representing conservation of number density, momentum and energy together with the transfer of solar radiation in the streams responsible for the major photolytic processes and the heating of the nucleus. The validity of the model is restricted to the collision-dominated region where all the gas species are assumed to attain a common velocity and common temperature. Two models are considered for the transfer of solar radiation through the circum-nuclear dust halo. In the first only the direct extinction by the dust is considered. In the second, the finding of some recent models, that the diffuse radiation field due to multiple scattering by the dust halo more or less compensates for radiation removed by direct absorption when the optical depth is near unity, is approximated by neglecting the attenuation of the radiation by the dust altogether.

As has been shown earlier, the presence of dust results in a transonic solution, and it is obtained by a two-step iterative procedure which makes use of the asymptotic behaviour of the radiation fields sufficiently far from the nucleus and a regularity condition at the sonic point.

The calculations were performed for a medium sized comet ($R_n = 2.5$ km) having a dust to gas production rate ratio of unity, at a heliocentric distance of 1 AU. The dust grains were assumed to be of the same radius (1 μ), of low density ($\rho \approx 1\,\mathrm{g\,cm^{-3}}$) and be strongly absorbing (having the optical properties of magnetite).

The main effect of the dust on the cometary atmosphere is dynamic. While the dust-gas coupling persists to about $20R_n$, the strong 'throat effect' of the dust friction on the gas causes the latter to go supersonic quite rapidly. Consequently the sub-sonic region around the nucleus is very thin, varying between 45 and 85 m in the two models considered. On the other hand, while this highly absorbing dust has a temperature substantially above that of the gas in the inner coma, heat exchange between them does not significantly change the temperature profile of the gas. This is because of the predominance of the expansion cooling, and even more importantly, the IR-cooling by H_2O, in the inner coma. Consequently, the gas temperature goes through a strong inversion, as in the dust-free case, achieving a temperature as low as about 6 K within about 50 km of the nucleus, before increasing to about 700 K at $r = 10^4$ km, due to the high efficiency of photolytic heating over the cooling process in the outer coma. The Mach number achieves a maximum value of about 10 at the distance of the temperature minimum, thereafter steadily decreasing to a value of about 2.5 at $r \approx 10^4$ km.

It is shown that while the dust attenuation has a strong effect on the production rate of H_2O, it also has an interesting effect on the electron density profile. It increases the electron density in the inner coma over the unattenuated case, while at the same time, decreasing it in the outer coma. In conclusion, the limitations of the present model and the necessity to extend it using a multi-fluid approach are discussed.

1. Introduction

In a previous paper (Marconi and Mendis, 1982a; hereafter referred to as Paper I) a self-consistent solution of the dynamic and thermal structure of an H_2O-dominated,

* Also Department of Physics.

† Also Department of Electrical Engineering and Computer Science.

The Moon and the Planets **27** (1982) 27–46. 0165–0807/82/0271–0027$03.00.

multispecies cometary atmosphere (at 1 AU) was obtained by numerically solving the simultaneous set of differential equations representing conservation of number density, momentum, energy and flux of UV radiation in three streams responsible for the major photolytic processes.

In that paper it was assumed that the cometary atmosphere was totally dust-free. This assumption led to two essential simplifications in the solution of the problem. Firstly, a purely supersonic solution could be assumed with the initial gas velocity at the nuclear surface being sonic. Secondly, the solar radiation which is responsible for heating the cometary nucleus (viz., the radiation in the visual and the near infrared, where most of the energy is contained) penetrates to the nucleus with negligible attenuation by the cometary atmosphere. Consequently, a simultaneous solution of the energy balance equation at the surface, together with the Clausius–Clapeyron equation for the sublimation of ice, gives the initial (surface) values for the temperature and number density of H_2O.

Photometric observations, however, indicate that cometary atmospheres are contaminated by dust. Following Whipple (1950) the cometary nucleus is generally envisaged as an admixture of frozen gases and dust. When such a 'dirty-snowball' approaches the sun the ices sublimate and the escaping gases will entrain some fraction of the smaller dust grains.

In this paper we will study the effect of this dust on both the dynamics and the thermodynamics of the cometary atmosphere in a self-consistent way.

The dynamical effects of the dust on the expanding gas was first discussed by Probstein (1968), who showed that the dust drag on the gas made its flow transonic, with the initial expansion speed from the nucleus being subsonic. Probstein, however, did not consider the effect of dust on the transfer of solar radiation, nor did he consider the external heating of the gas and dust and the exchange of heat between them.

Weissman and Kieffer (1981) has recently considered the effect of circum-nuclear dust in the transfer of solar radiation to the nucleus, taking into account the effect of both direct absorption and multiple scattering. But this treatment does not consider the dynamical effects of the dust on the gas. Its main aim was to derive the temperature profile of the cometary nucleus, and the associated production rates of cometary volatiles. A more self-consistent model of a dusty cometary atmosphere is due to Hellmich (1979, 1981), who combined the radiative transfer of solar radiation through the circum-nuclear dust with the two-phase gas-dust hydrodynamics of Probstein (1968). Hellmich, however, does not consider the photochemical heating of the cometary gas, the radiative heating of the dust, and the transfer of heat between them. His main concern is to demonstrate the influence of the radiation transfer in the circum-nuclear dust on the production rates of gas and dust from the nucleus.

In this paper we attempt a self-consistent solution of the dynamical and thermal structure of an H_2O-dominated, multispecies cometary atmosphere, which also contains dust. We will take into account the proper photochemical heating of the gas, the radiative heating of the dust and the exchange of heat between them, and we will construct the

radial profiles of all the thermodynamic and flow parameters of the gas and the dust, throughout the collision dominated region of the transonic cometary atmosphere.

Our treatment is limited by the fact that it does not take into account multiple scattering. We therefore consider two different models. The first considers only direct extinction by the dust. In the second, we ignore the attenuation of the radiation by the dust altogether. We expect that this simple model reasonably approximates the multiple scattering situation when the optical depth of direct extinction by the dust, $\tau_0 \approx 1$ (as is the case for a typical medium bright comet at a heliocentric distance of 1 AU). This is based on the results of Hellmich (1981) and by Wiessman and Kieffer (1981), namely that the diffuse radiation field due to multiple scattering approximately compensates for the direct absorption by the dust when $\tau_0 \approx 1$.

2. The Model

2.1. PHOTOCHEMISTRY

In paper I, we pointed out that there are good reasons to believe that the main volatile constituent of at least some cometary nuclei, if not a majority is H_2O-ice. In this paper, too, we will minimize the chemistry by assuming that the only ice species present in the nucleus is H_2O. The only difference here is that, unlike in paper I, we will assume that the nucleus also contains a component of non-volatile dust embedded in the ice. As we argued in paper I, the addition of small mole fractions of other species, particularly CO, CO_2, and N_2, while significantly altering the chemical profile of the cometary atmosphere, is not expected to alter the temperature and velocity profile there. This is because, as long as H_2O is the predominant constituent in the atmosphere, its heating will be dominated by the UV photolysis of H_2O. Furthermore, while other likely species could act as good coolants of the cometary atmosphere, it is noted that H_2O is a highly polar molecule, whose large dipole moment renders it a very efficient emitter in the infrared. Consequently, to a first order we may assume that the H_2O molecule plays the dominant role both in the heating and in the cooling of the cometary atmosphere. In the present case, of course, the effect of dust in the thermodynamics of the atmosphere is also included.

Even with a pure H_2O nucleus, the number of chemical species that have to be considered is substantial. In the course of its outflow from the nucleus H_2O is photo-destructed into such species as OH, O, H, O^+, H^+, H_2O^+, etc. These in turn react with one another, yielding such species as H_3O^+, O_2^+, H_3^+, etc. The chemical species that are considered in this model are (as in Paper I) H_2O, OH, H, O, H_2, O_2, H_3O^+, H_2O^+, OH^+, O^+ and H^+. Other possibilities such as H_2^+, H_3^+, HO_2^+, and O_2^+ are neglected, because these are formed relatively slowly by the photolytic products of H_2O and then rapidly destroyed by direct reactions with H_2O. Their importance to the energetics of the cometary atmosphere is therefore likely to be small.

All the chemical reactions considered in our model, along with their rate constants at 1 AU are listed in Table I. Also included with each reaction is the energy release when available, and the reaction threshold where applicable.

TABLE I

Chemical processes in a H_2O-atmosphere

	Reaction		Energy release (eV)	Threshold (Å)	Rate**	Reference
(1)	$H_2O + h\nu$	$\rightarrow OH + H$	1.9	1860	1.02×10^{-5}	HC 80
(2)		$\rightarrow H_2 + O(^1D)$	1.9	1450	1.35×10^{-6}	HC 80
(3)		$\rightarrow H_2O^+ + e$	12.3	984	3.34×10^{-7}	HC 80
(4)		$\rightarrow OH + H^+ + e$	25	662	1.2×10^{-8}	HC 80
(5)		$\rightarrow H_2 + O^+ + e$	36.3	665	5.8×10^{-9}	HC 80
(6)		$\rightarrow H + OH^+ + e$	18.5	684	5.5×10^{-8}	HC 80
(7)	$H_2O + O(^1D)$	$\rightarrow OH + OH$	1.26		3×10^{-10}	BK 73
(8)	$H_2O + H_2O^+$	$\rightarrow H_3O^+ + OH$	1.1*		2.05×10^{-9}	H 80
(9)	$H_2O + OH^+$	$\rightarrow H_3O^+ + O$	1.82+		1.3×10^{-9}	H 80
(10)		$\rightarrow H_2O^+ + OH$	–		1.6×10^{-9}	H 80
(11)	$H_2O + H^+$	$\rightarrow H_2O^+ + H$	–		8.2×10^{-9}	PH 80
(12)	$H_2O + O^+$	$\rightarrow H_2O^+ + O$	–		2.3×10^{-9}	PH 80
(13)	$OH + h\nu$	$\rightarrow O + H$	0.4 ~ 2.0†	~ 2800†	5×10^{-6}	HG 80
(14)	$OH + OH$	$\rightarrow H_2O + O$	0.74+		$4.9 \times 10^{-11} \exp(-400/T)$	BGH 81
(15)	$OH + O$	$\rightarrow O_2 + H$	0.73+		$4 \times 10^{-11} (T/300)^{1/2}$	PH 80
(16)	$OH + H_2O^+$	$\rightarrow H_3O^+ + O$	?		6.9×10^{-10}	PH 80
(17)	$OH + OH^+$	$\rightarrow H_2O^+ + O$	?		7×10^{-10}	PH 80
(18)	$H_2 + OH^+$	$\rightarrow H_2O^+ + H$	1.19+		1.05×10^{-9}	PH 80
(19)	$O_2 + h\nu$	$\rightarrow O_2^+ + e$	17.2	1028	5.1×10^{-7}	HC 80
(20)		$\rightarrow O + O$	1.3	1759	4.2×10^{-6}	HC 80
(21)	$H_3O^+ + e$	$\rightarrow OH + H_2$	6.4*		$2.33 \times 10^{-7} (T/300)^{-1/2}$	BGH 81
(22)		$\rightarrow OH + H + H$	1.2*		$2.33 \times 10^{-7} (T/300)^{-1/2}$	BGH 81
(23)		$\rightarrow H_2O + H$	6.4*		$2.33 \times 10^{-7} (T/300)^{-1/2}$	BGH 81
(24)	$H_2O^+ + e$	$\rightarrow OH + H$	7.5*		$5.32 \times 10^{-7} (T/300)^{-1/2}$	BGH 81
(25)		$\rightarrow O + H_2$	7.5*		$1.5 \times 10^{-7} (T/300)^{-1/2}$	BGH 81
(26)	$H_2O^+ + H_2$	$\rightarrow H + H_3O^+$	1.82		1.4×10^{-9}	BK 73
(27)	$OH^+ + e$	$\rightarrow O + H$	?		$2 \times 10^{-7} (T/300)^{-1/2}$	PH 80

** The photo-reaction rates have units of s^{-1}, whereas the chemical reaction rates have units of $cm^3\ s^{-1}$.

(Energy release and threshold values correspond to given references unless otherwise indicated by + or *. + refers to BK73, * refers to S. S. Prasad, private communication, † refers to W. M. Jackson, private communication.)

The abbreviations for the references stand for the following:

HC 80: Huebner, W. F. and Carpenter, C. W., 1980, *Los Alamos Scientific Laboratory Report*, LA-8085-MS.

BGH 81: Biermann, L. and Giguere, P. T., 1981, *Los Alamos Scientific Laboratory Report*, LA-UR-81-1335.

H 80: Huntress, W. T. Jr., McEwan, M. J., Kierpas, Z. and Anicich, V. G., 1980, *Astrophys. J. Suppl. Ser. 44*, 481.

BK 73: Banks, P. M. and Kockarts, G., 1973, *Aeronomy*, Academic Press, N.Y.

PH 80: Prasad, S. S. and Huntress, W. T. Jr., 1980, *Astrophys. J. Suppl. Ser. 42.*

2.2. RADIATIVE TRANSFER

As pointed out in Paper I, the most important photolytic processes associated with the absorption of solar UV radiation in the cometary atmosphere are:

$$\textcircled{1} \qquad H_2O + h\nu \rightarrow OH + H, \lambda \leqslant 1860\,\text{Å}.$$

$$\textcircled{2} \qquad H_2O + h\nu \rightarrow H_2 + O(^1D), \lambda \leqslant 1450\,\text{Å}.$$

$$\textcircled{3} \qquad H_2O + h\nu \rightarrow H_2O^+ + e, \lambda \leqslant 984\,\text{Å}.$$

Corresponding to the above reactions we will divide the solar UV flux in the range $0 \leqslant \lambda \leqslant 1860$ Å into 3 streams, J_1, J_2 and J_3, where J_1 is the photon flux in the range $1450\,\text{Å} < \lambda \leqslant 1860\,\text{Å}$, J_2 is the photon flux in the range $984\,\text{Å} < \lambda \leqslant 1450$ Å and J_3 is the photon flux in the range $0 < \lambda \leqslant 984$ Å.

In the dust-free H_2O-cometary atmosphere treated in Paper I this UV radiation would be largely attenuated only by these photolytic processes. At the same time the bulk of the radiant energy from the sun, which is concentrated in the visual and near-IR, penetrates to the nucleus with negligible attenuation by the cometary gases. In the presence of dust, the situation is quite different. The dust attenuates both the solar UV flux as well as the radiant energy in the visual and near-IR.

In order to calculate the extinction of the solar radiation by the dust, we need not only the density and radial distribution of the dust, but also the nature and size distribution of the dust. The latter parameters are known only rather imperfectly (e.g., see Hanner, 1980, for an excellent review of the subject). In fact, observations of the brightness and polarization of the scattered sunlight, the thermal emission, the broad IR features around 19 and 20μ, and the ratio of the solar radiation pressure to solar gravity (inferred from the grain dynamics), cannot all be explained by the same type of grain. In fact, the best candidate appears to be fluffy, low bulk density material that is also highly absorbing. Silicates contaminated with significant amounts of absorbing material such as magnetite may explain most of these features, including the far-IR features (Hanner, 1980). For the purpose of our calculation, we assume a low bulk density ($\rho \approx 1\,\text{g cm}^{-3}$) grain with the optical properties of magnetite. The size distribution of the dust, which is derived from dynamical analysis of dust tails and which is model dependent indicates a rather peaked distribution with low radius cut-off around 0.45μ when $\rho \approx 1\,\text{g cm}^{-3}$ (Sekanina and Miller, 1973). In this study we will, for convenience, assume a single grain size (radius, $a = 1\mu$).

Dust of this assumed size and composition strongly absorbs and scatters radiation in the neighborhood of the solar spectral maximum. As a result, the insolation and in turn, the production rate of gas (and dust) from the comet may be strongly effected. Consequently, the radiative transfer of the total solar energy flux I ($0 \leqslant h\nu < \infty$) due to the dust will also be considered.

For all the four streams ($J_i, i = 1, 2, 3$; and I) only direct extinction is calculated. For the case of I, an attempt will be made to include the effects of multiple scattering by the dust, with a second, highly simplified model. Also, as in Paper I, we assume the cometary

atmosphere to be spherically symmetric. The inclusion of the radiation field, which has rotational symmetry about the sun-comet axis, destroys the aforementioned spherical symmetry. It is, however, beyond the scope of the present paper to incorporate this effect, and we still assume spherically symmetric flow. This simplification essentially restricts the validity of our computed profiles to the sun-comet axis.

Since the size of the cometary atmosphere is very much smaller than the heliocentric distance of the comet, there is no appreciable divergence of the solar radiation across it and so can be considered plane parallel. We then have

$$\frac{\mathrm{d}J_i}{\mathrm{d}r} = \left(\sum_{j=1}^{3} \bar{\sigma}_{ji} n_{\mathrm{H_2O}} + \bar{q}_{i,\mathrm{ext}}\, \pi a^2 n_d \right) J_i, \tag{1}$$

$$\frac{\mathrm{d}I}{\mathrm{d}r} = \bar{q}_{0,\mathrm{ext}}\, \pi a^2 n_d I, \tag{2}$$

where $J_i (1 \leqslant i \leqslant 3)$ is the solar UV radiation in the i-th stream at a nuclear distance r, $n_{\mathrm{H_2O}}$ is the number density of H_2O, $\bar{\sigma}_{ji}$ is the average photo-destruction cross-section of H_2O in the j-th photolytic process by the i-th stream, n_d is the number density of dust of radius $a (= 1\mu)$, $\bar{q}_{i,\mathrm{ext}}$ is the mean efficiency of extinction of the solar UV radiation in the i-th stream by the dust, I is the total solar energy flux (ergs cm^{-2} s^{-1}) and $\bar{q}_{0,\mathrm{ext}}$ is the associated mean efficiency of extinction by the dust.

The values of $\bar{\sigma}_{ji}$ were calculated from the tabulations of the variations of σ_j with λ given in Huebner (1981). They are (in units of cm^2) the following: $\bar{\sigma}_{11} = 2.6 \times 10^{-18}$, $\bar{\sigma}_{12} = 2.9 \times 10^{-18}$, $\bar{\sigma}_{13} = 2.9 \times 10^{-18}$, $\bar{\sigma}_{22} = 2.4 \times 10^{-18}$, $\bar{\sigma}_{23} = 1.0 \times 10^{-18}$, $\bar{\sigma}_{33} = 8.4 \times 10^{-18}$, $\bar{\sigma}_{21} = \bar{\sigma}_{31} = \bar{\sigma}_{32} = 0$. Also $\bar{q}_{i,\mathrm{ext}}$ $(i = 0, 1, 2, 3)$ is given by

$$\bar{q}_{i,\mathrm{ext}} = \frac{\int_{\lambda_i} q_{\mathrm{ext}}(a, \lambda, m(\lambda)) S_{\odot}(\lambda)\, \mathrm{d}\lambda}{\int_{\lambda_i} S_{\odot}(\lambda)\, \mathrm{d}\lambda}, \tag{3}$$

where the extinction coefficient, q_{ext} as a function of wavelength λ, complex index of refraction, m, and grain radius, a, was computed for magnetite according to Mie theory (van de Hulst, 1981). The complex index of refraction $m(\lambda)$ was obtained from Huffman (1982), and the solar spectral energy density $S_{\odot\lambda}$ is obtained from Allen (1976). The range of integration in the four cases (0, 1, 2, 3) are clearly $(0 - \infty)$, (1450–1860 Å), (984–1450 Å), and (0–984 Å), respectively. The result of the integration is, $\bar{q}_{0,\mathrm{ext}} \approx 2.44$, $\bar{q}_{1,\mathrm{ext}} \approx 2.15$, $\bar{q}_{2,\mathrm{ext}} \approx 2.10$, $\bar{q}_{3,\mathrm{ext}} \approx 2.00$.

The integration of (1) and (2) yield

$$J_i(r) = J_i(\infty) \exp - \left(\sum_{j=1}^{3} \bar{\sigma}_{ji} \int_r^{\infty} n_{\mathrm{H_2O}}\, \mathrm{d}r + \bar{q}_{i,\mathrm{ext}}\, \pi a^2 \int_r^{\infty} n_d\, \mathrm{d}r \right) = J_i(\infty)\, e^{-\tau_i(r)}, \tag{4}$$

$$I(r) = I(\infty) \exp\left(-\bar{q}_{0,\text{ext}}\, \pi a^2 \int_r^\infty n_d \, dr\right) = I(\infty)\, e^{-\tau_0(r)}, \tag{5}$$

where $J_i(\infty)$ is the unattenuated flux ($\text{cm}^{-2}\,\text{s}^{-1}$) in the i-th UV stream, $I(\infty)$ is the total unattenuated solar radiant energy flux ($\text{erg}\,\text{cm}^{-2}\,\text{s}^{-1}$), and $\tau_i(r)$ is the mean optical depth in the i-th stream at a nuclear distance of r.

Finally, the values of $J_i(\infty)$ and $I(\infty)$ at a heliocentric distance d AU are given by

$$\left.\begin{aligned} J_i(\infty) &= J_i^{(1)}(\infty) d^{-2}, \\ I(\infty) &= I^{(1)}(\infty) d^{-2}; \end{aligned}\right\} \tag{6}$$

where $J_i^{(1)}(\infty)$ and $I^{(1)}(\infty)$ are the unattenuated fluxes in the four streams at 1 AU and are given by: $J_1^{(1)}(\infty) = 3.5 \times 10^{12}\ \text{cm}^{-2}\,\text{s}^{-1}$, $J_2^{(2)}(\infty) = 4.2 \times 10^{11}\ \text{cm}^{-2}\,\text{s}^{-1}$, $J_3^{(1)}(\infty) = 4.5 \times 10^{10}\ \text{cm}^{-2}\,\text{s}^{-1}$ and $I^{(1)}(\infty) = 1.35 \times 10^6\ \text{erg}\,\text{cm}^{-2}\,\text{s}^{-1}$.

As we have already stated, Hellmich (1979, 1981) as well as Weissman and Kieffer (1981) have investigated the effects of multiple scattering by the dust in the cometary atmosphere. They find that for dust optical depths ~ 1 (which are typically reached around 1 AU for an average comet), multiple scattering by the dust, may more than compensate for the effects of direct extinction. The reason for this is that the extended halo of dust around the nucleus, provides a large collecting area for the incoming solar radiation. Our present model does not take into account multiple scattering, but we attempt to simulate it with a very simple approximation, in a second model. There it is assumed that the diffuse radiation reaching the nucleus due to multiple scattering by dust exactly compensates for the radiation removed by direct absorption and single scattering (i.e., extinction). Consequently, in this model, the extinction of the solar radiation by the dust is neglected altogether.

2.3. Dynamics

As we pointed out in Paper I, the time scale for changes in the comet's heliocentric distance is typically much larger than the characteristic time scales for photodestruction and flow within the cometary atmosphere. Consequently, we assume a quasi-steady, spherically symmetric expansion of the gas-dust mixture. Intermolecular collisions are sufficiently efficient up to about 10^4 km to make the multispecies gas component behave as a single fluid, having the same velocity and temperature (see Paper I).

For a given gas species denoted by the subscript i, the continuity equation is given by

$$\frac{1}{r^2} \frac{\mathrm{d}}{\mathrm{d}r} (r^2 n_i u_g) = S_i, \tag{7}$$

where n_i is the number density, u_g is the single fluid gas velocity and S_i is the net source term ($\text{cm}^{-3}\,\text{s}^{-1}$), which is calculated using the appropriate photolytic and chemical reaction rates listed in Table I. For the dust component, having number density n_d and velocity u_d, the corresponding continuity equation is,

$$\frac{1}{r^2}\frac{\mathrm{d}}{\mathrm{d}r}(r^2 n_d u_d) = 0. \tag{8}$$

The 1-fluid momentum equation for the gas is given by

$$\rho_g u_g \frac{\mathrm{d}u_g}{\mathrm{d}r} = -\frac{\mathrm{d}P}{\mathrm{d}r} - F_{dg}, \tag{9}$$

where P is the one-fluid pressure (which is the sum of all partial pressures), ρ_g ($= \Sigma_i n_i m_i$) is the total gas mass density and F_{dg} is the drag exerted by the expanding gas on the entrained dust.

The gas collisional mean free path ($\gtrsim 1$ m) is much larger than the grain size ($\sim 1\mu$). Consequently, from the point of view of the dust the gas flow is 'free-molecular'. The free-molecular gas drag on the dust has been calculated by Probstein (1968), by integrating the net gas momentum flux to grain, over its surface, assuming a drifting-Maxwellian velocity distribution, and total accommodation on the surface. It is given by

$$F_{dg} = \tfrac{1}{2} C_D \cdot \pi a^2 \rho_g (u_g - u_d)^2 n_d, \tag{10}$$

with the free-molecular 'drag-coefficient' C_D, given by

$$C_D = \frac{2}{3}\frac{\sqrt{\pi}}{\omega}\sqrt{\frac{T_d}{T_g}} + \frac{2\omega^2 + 1}{\sqrt{\pi}\omega^3} e^{-\omega^2} + \frac{4\omega^4 + 4\omega^2 - 1}{2\omega^4}\,\mathrm{erf}\,(\omega), \tag{11}$$

where T_g and T_d are the gas and dust temperature, respectively; and

$$\omega = (u_g - u_d) \Big/ \sqrt{\frac{2kT_g}{\bar{m}}}, \tag{12}$$

where $\bar{m}$ is the mean mass of a gas molecule and k is Boltzmann's constant.

Analogously, the conservation of momentum for the dust component is given by

$$\rho_d u_d \frac{\mathrm{d}u_d}{\mathrm{d}r} = F_{dg}, \tag{13}$$

where it is noted that the inter-dust particle collision rate, and therefore the 'dust partial pressure' is negligible.

The 1-fluid energy equation for the gas may be written as

$$\frac{1}{r^2}\frac{\mathrm{d}}{\mathrm{d}r}\left[r^2 \rho_g u_g \left(h_g + \tfrac{1}{2}u_g^2\right)\right] = \dot{Q}_g - \dot{L}_g + \dot{Q}_{dg} - u_d F_{dg}, \tag{14}$$

where h_g is the specific gas enthalpy, $\dot{Q}_g$ is the energy density production rate via chemical and photochemical processes, $\dot{L}_g$ is the energy density loss rate due to radiative cooling, $\dot{Q}_{dg}$ is the heat exchange rate between the gas and the dust and the last term corresponds to the (reversible) work done by the gas in accelerating the dust. As we showed in Paper I, the thermal conductivity term: $1/r^2\ \mathrm{d}/\mathrm{d}r(r^2 K\ \mathrm{d}T_g/\mathrm{d}r)$ may be neglected.

The gas enthalpy is assumed to be due to the most abundant species H_2O, OH, and H, with, according to Zucrow and Hoffman (1976),

$$h_{H_2O} = \int_0^{T_g} C_{P,H_2O}(T)\,dT = \frac{k}{m_{H_2O}}(4.07T_g - 5.56 \times 10^{-4}\,T_g^2 + \\ + 1.38 \times 10^{-6}\,T_g^3 - 7.4 \times 10^{-10}\,T_g^4 + 1.60 \times 10^{-13}\,T_g^5), \quad (15)$$

$$h_{OH} = \frac{3.62kT_g}{m_{OH}}, \quad (16)$$

$$h_H = \frac{2.5kT_g}{m_H}; \quad (17)$$

and

$$h = \sum_{i=H_2O,OH,H} n_i m_i h_i \Big/ \sum_{i=H_2O,OH,H} n_i m_i \approx \frac{1}{\rho_g} \sum_{i=H_2O,OH,H} n_i m_i h_i. \quad (18)$$

Equation (16) is accurate to within a few percent over the temperature range 100–1000 K, which, as we will see later, encompasses much of the temperature range in the cometary atmosphere.

The source term for the energy production rate via chemical and photochemical processes, $\dot{Q}_g$ is given by

$$\dot{Q}_g = \sum_{\text{all reactions}} R_i \epsilon_i, \quad (19)$$

where R_i is the i-th reaction rate constant (in $cm^{-3}\,s^{-1}$) and ϵ_i is the mean energy release in that reaction (see Table I). This term includes contributions from the UV photolytic heating as well as exothermic chemical reactions. In particular, the fast photolytic processes ①, ②, ③, and ⑬, and the efficient exothermic processes ⑦, ⑧, ⑨, ⑭, ㉑, ㉒, ㉓, ㉔, and ㉕ of Table I are included. The neglect of the remaining processes is justified due to their comparative slowness.

With regard to the loss term for the energy density $\dot{L}_g$ in Equation (14), we follow Shimizu (1975, 1976) in assuming that it largely results from infrared emissions due to rotational transitions in the highly polar molecule, H_2O. As in Paper I, we use Shimizu's (1976) empirical formula; viz.,

$$\dot{L}_g = \frac{8.5 \times 10^{-19}\,T_g^2 n_{H_2O}^2}{n_{H_2O} + 2.7 \times 10^7\,T_g} (\text{erg cm}^{-3}\,\text{s}^{-1}), \quad (20)$$

which reduces to the LTE cooling rate of $\dot{L}_i = 8.5 \times 10^{-19}\,n_{H_2O} T_g^2$ in the inner coma ($r \leqslant 10^2$ km) and to the non-LTE value of $\dot{L}_0 \simeq 3.1 \times 10^{-26}\,n_{H_2O}^2 T_g$ in the outer coma ($r \geqslant 10^3$ km).

The heat exchange term, $\dot{Q}_{dg}$, in Equation (14) is also given by Probstein (1968), as

$$\dot{Q}_{dg} = 4\pi a^2 \cdot \text{St} \cdot C_p \rho_g (u_g - u_d)(T_d - T_r) n_d, \quad (21)$$

where St is the 'Stanton-number' given by

$$\mathrm{St} = \frac{\gamma+1}{8\gamma\omega^2}\left[\frac{1}{\sqrt{\pi}}\,\omega\, e^{-\omega^2} + (\omega^2+\tfrac{1}{2})\,\mathrm{erf}\,(\omega)\right]; \tag{22}$$

T_r is the 'recovery temperature' given by

$$T_r = \frac{T_g}{\gamma+1}\left[2\gamma + 2(\gamma+1)\omega^2 - \frac{\gamma-1}{\frac{1}{2}+\frac{1}{\omega^2}+\frac{\omega}{\sqrt{\pi}\,\mathrm{erf}\,(\omega)}\,e^{-\omega^2}}\right], \tag{23}$$

and $\gamma = C_p/(C_p - k/\bar{m})$, is the ratio of specific heats for the gas mixture, with the specific heat at constant pressure for the gas mixture, C_p, being given by

$$C_p = \sum_{i=\mathrm{H_2O,\,OH,\,H}} C_{pi} n_i m_i \Big/ \sum_{i=\mathrm{H_2O,\,OH,\,H}} n_i m_i \approx \frac{1}{\rho_g} \sum_{i=\mathrm{H_2O,\,OH,\,H}} C_{pi} n_i m_i. \tag{24}$$

The energy equation for the dust component is given by

$$\rho_d u_d C_d \frac{\mathrm{d}T_d}{\mathrm{d}r} = -\dot{Q}_{dg} + \dot{Q}_{\mathrm{rad}}, \tag{25}$$

where

$$\dot{Q}_{\mathrm{rad}} = q_{\odot,\,\mathrm{abs}}\pi a^2 I(r) n_d - q_{\mathrm{emit}}(T_d) \times 4\pi a^2 \times \sigma T_d^4 n_d, \tag{26}$$

with

$$q_{\odot,\,\mathrm{abs}} = \int_0^\infty Q_{\mathrm{abs}}(\lambda, m, a) S_\odot(\lambda)\,\mathrm{d}\lambda \Big/ \int_0^\infty S_\odot(\lambda)\,\mathrm{d}\lambda \approx 1.1,$$

$$q_{\mathrm{emit}}(T_d) = \int_0^\infty Q_{\mathrm{abs}}(\lambda, m, a) \times \pi B(\lambda, T_d)\,\mathrm{d}\lambda/\sigma T_d^4; \tag{27}$$

where $B(\lambda, T_d)$ is the black-body energy spectral distribution at temperature T_d and σ is the Stephan–Boltzmann constant ($= 5.67 \times 10^{-5}$ erg cm^{-2} s^{-1} K^{-4}).

The specific heat capacity $C_d(T)$ for magnetite is contained in the JANAF Tables (1971), and may be fitted by the expression

$$C_d(T) = 7.78 \times 10^7 - 1.59 \times 10^6\, T_d + 1.39 \times 10^4\, T_d^2 - \\ - 48.0 T_d^4 + 9.65 \times 10^{-3}\, T_d^4 - 7.08 T_d^5. \tag{28}$$

Finally, the set of equations, given above, is closed by the perfect gas equation for the 1-fluid atmosphere, by requiring that

$$P = nkT_g; \tag{29}$$

(where $n = (\Sigma_i n_i)$ is the total number density), together with the constraint that the dust to gas production rate ratio χ is fixed; i.e.,

$$\rho_d u_d = \chi \rho_g u_g. \tag{30}$$

3. Numerical Procedure

The set of equations (1), (2), (7), (8), (9), (13), (14), and (25) may be recast explicitly as a set of first-order, non-linear differential equations relating the radial gradients in the flow and radiation fields to the flow and radiation fields themselves. Such an assembly of simultaneous differential equations (together with the constitutive equations) has a unique solution if an appropriate set of boundary conditions is provided. In the problem considered here the asymptotic behavior of the attenuation coefficients ($e^{-\tau_i}$) and the behavior of the gradient of the Mach number at the sonic point constitute such a set. To be more specific, a solution is sought, in which $e^{-\tau_i} \sim 1$ at any boundary sufficiently removed from the nucleus, that the solar flux may be assumed to be unattenuated. Moreover, since the dust exerts an appreciable drag on the gas near the nuclear surface, the initial Mach number < 1, and the proper solution is the singular one which smoothly traverses the sonic point r_* having $dM/dr = 0$ (i.e., a saddle point) there (Probstein, 1968). Clearly a full set of boundary conditions are unavailable at any one boundary and consequently an iterative process must be employed to arrive at the solution.

A two stage iterative procedure is adopted to this end. A significant simplification is allowed by the insensitivity of the dynamics in the innermost region to the UV radiation field and the associated chemistry. Consequently as a first tep a self-consistent solution is obtained for the dust-H_2O gas mixture alone (all other molecular species being ignored). While this solution is valid only near the nuclear surface, it is sufficient to provide the boundary conditions on the surface required for the next step.

To begin with an initial surface Mach number M_S (< 1), and an initial $I(r)$ (taken to be constant as the first guess) are assumed. It is then possible to calculate the surface values of the remaining flow variables (T_g, $n(H_2O)$, u_g, T_d, n_d, u_d). To this end we use the energy-balance equation at the surface

$$\frac{1-A_S}{d^2} I(r_N) \langle \cos\theta \cos\phi \rangle + \bar{I}_{\mathrm{Diff}} = \epsilon_S \sigma T_S^4 + \frac{L}{N_A} \dot{Z}. \tag{31}$$

The Clausius–Clapeyron equation

$$n_S(H_2O) = n_0 \left(\frac{T_0}{T_S}\right) \exp\left[-\frac{L}{kN_A}\left(\frac{1}{T_S} - \frac{1}{T_0}\right)\right]; \tag{32}$$

and the energy-balance for the dust at the surface

$$-\dot{Q}_{dg} + \dot{Q}_{\mathrm{rad}} = 0. \tag{33}$$

In the above equations $\langle \cos\theta \cos\phi \rangle = 1/4$, where θ and ϕ are the local hour angle and latitude, A_S is the surface bolometric albedo (≈ 0.63), ϵ_S is the surface IR-emissivity (~ 0.37) (e.g., see Houpis and Mendis, 1981), L is the latent heat of sublimation of H_2O ($\approx 5.0 \times 10^{11}$ ergs/mole), N_A is Avogadro's number ($\approx 6.0 \times 10^{23}$), $T_0 = 373$ K and $n_0 = 1.94 \times 10^{19}$ cm^{-3}. Also the diffuse radiation reaching the surface, $\bar{I}_{\mathrm{Diff}}$, is neglected. Finally, the production rate $\dot{Z}$ of H_2O at the surface, is given by

$$\dot{Z} = n_S(H_2O)u_{gS} = n_S(H_2O)M_S\left(\frac{\gamma_{H_2O}kT_S}{m_{H_2O}}\right)^{1/2}. \quad (33)$$

At the surface u_d is assumed to be arbitrarily small. In our model we take $u_d \approx 1\,\mathrm{ms}^{-1}$, since $u_d = 0$, leads to a singularity in the dust density at the surface. The dust density is then calculated from Equation (30) taking the dust to gas ratio $\chi = 1$.

With these boundary values determined from the guesses for M_S and $I(r)$, an outward integration is performed. This sequence is repeated until for some choice of M_S, $\mathrm{d}M/\mathrm{d}r \approx 0$ (to some acceptable tolerance) at $M = 1$. Having obtained this solution, which traverses the sonic point smoothly (i.e. the transonic solution) the integration is continued beyond the sonic point to the outer boundary of our model ($r \approx 2.5 \times 10^4$ km). From this solution a new, improved $I(r)$ is calculated, using Equation (5), and the search for the new transonic solution consistent with this improved radiation field is instituted. Finally, when the $I(r)$ obtained from successive iterations are sufficiently close, the procedure is terminated.

In the second step the chemistry is introduced and a solution that is self-consistent with the UV radiation fields J_i ($i = 1, 2, 3$) is sought. To do this we start with the values of n_{H_2O} and n_d of the previous step and the corresponding $J_i(r)$ are computed from Equation (4). These $J_i(r)$ are then employed to determine the new photolytic coefficients and hence a new solution. The procedure is repeated until these radiation fields in successive iterations are sufficiently close. In fact, the convergence in this phase is extremely rapid, so that the self-consistent J_i ($i = 1, 2, 3$) are fixed with only a few iterations.

4. Results and Discussion

As we stated earlier, we have considered two different models. In the first, only the direct extinction by the dust is considered. We will hereafter refer to this as the DE-model. In the second, the effect of multiple scattering by the dust is approximated in a very simple way by assuming that the diffuse radiation due to multiple scattering exactly compensates for the extinction of the direct solar radiation (i.e. we take $I(r) =$ constant). This pseudo-multiple scattering simulation model will hereafter be referred to as the PMS-model.

In the calculation, we have considered a medium bright comet such as P/Halley with radius $R_n = 2.5$ km. We have also restricted ourselves to the single heliocentric distance of 1 AU, and assumed the comet to be 'dusty' in taking $\chi = 1$. The results of the calculation are given in the following figures. In all these figures, the dotted lines represent the DE-model, while the solid lines refer to the PMS-model. The profiles of the gas and dust densities in the subsonic region are shown in Figure 1. All the lines terminate at the distance of the sonic point. It is seen that the subsonic region is very thin. It is only 45 m wide in the DE-model, while it is 85 m wide in the PMS-model. Just as it was shown by Probstein (1968), the dust-gas coupling persists till about 50 km (i.e., about 20 cometary radii). This is clear from Figure 5, where at this distance, the dust is seen to reach its terminal velocity. However, the strong 'throat effect' of the dust friction, in the

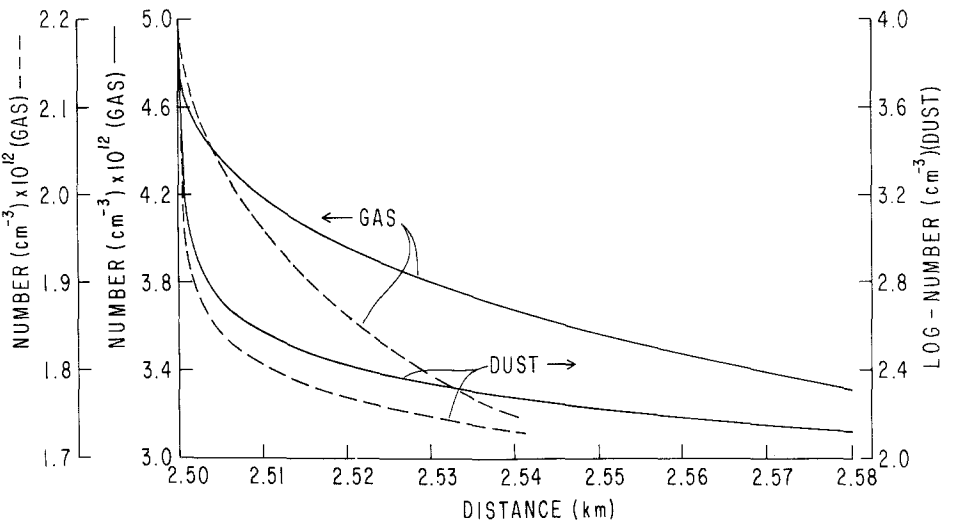

Fig. 1. Radial profiles of the number density of gas (H_2O) and dust in the subsonic region. Solid lines correspond to the PMS-model while broken lines correspond to the DE-model. All lines terminate at the distance of the sonic point.

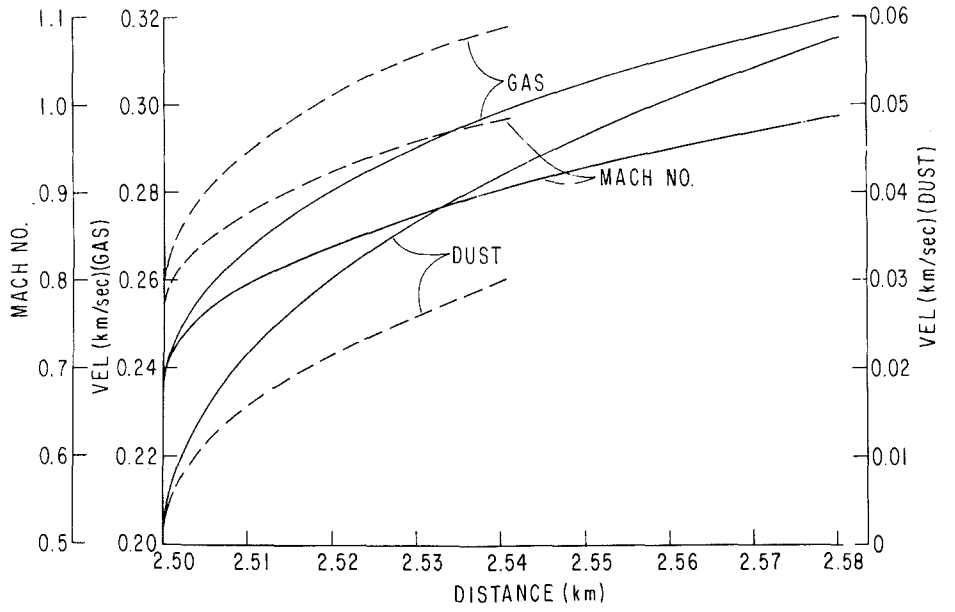

Fig. 2. Radial profiles of the Mach number, the gas velocity and the dust velocity in the subsonic region. Solid lines correspond to the PMS-model while the dotted lines correspond to the DE-model. All lines terminate at the distance of the sonic point.

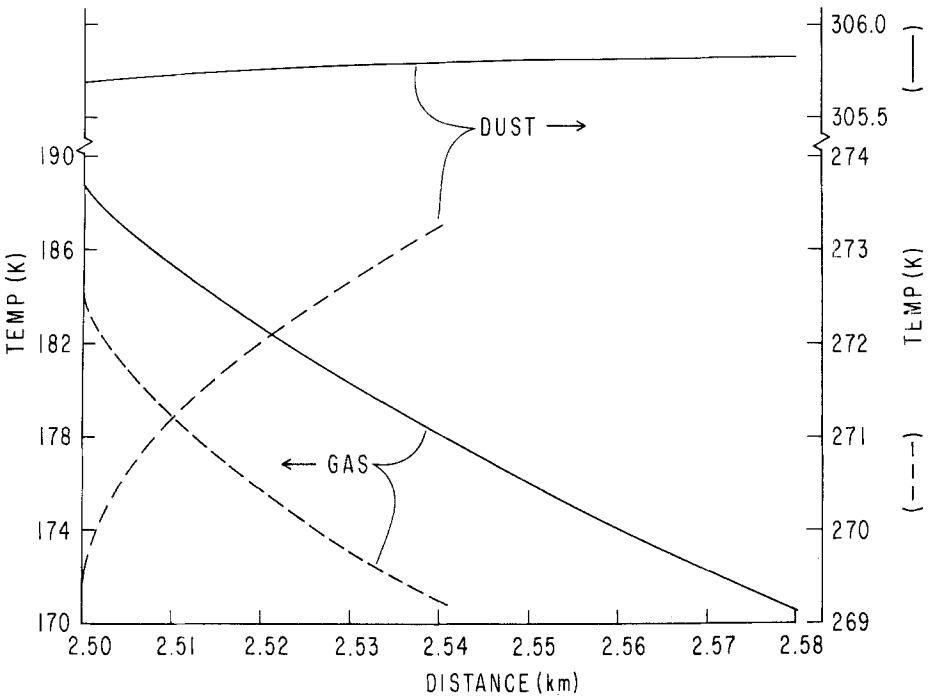

Fig. 3. Radial profiles of the temperature of gas and dust in the subsonic region. Solid lines correspond to the PMS-model while the broken lines correspond to the DE-model. All lines terminate at the distance of the sonic point.

subsonic region, causes the Mach number of the gas to increase rapidly and reach unity very close to the nucleus. Also, it is seen that in the PMS-model the gas (and therefore the dust) production rate is more than a factor of 2 larger than that in the DE-model. This is simply due to the larger amount of radiation reaching the nuclear surface in the former case.

The variations of the Mach number, and the gas and dust velocities in the subsonic region, are shown in Figure 2. It is seen that the initial Mach number in the PMS-model (≈ 0.69) is somewhat smaller than that in the DE-model (≈ 0.76). This is once again due to the larger production rate of dust in the former case, which causes the initial gas velocity to be smaller, while at the same time increasing the gas temperature (see Figure 3). The gas temperature, and therefore the sonic speed, is greater in the PMS-model due to the larger amount of solar radiation reaching the nucleus. The variation of gas and dust temperature in the subsonic region is shown in Figure 3. It is seen that the dust temperature is always considerably larger than the gas temperature. Also in the PMS-model, while the gas temperature decreases rapidly from about 188.5 K near the nucleus to about 171 K at the sonic point, the dust temperature changes hardly at all, remaining close to 306 K all the time. In the DE-model, while the gas temperature drops from about 184 K near the nucleus to about 171 K at the sonic point, the dust increases

from about 269.5 K to about 273.5 K in the same range. This decrease of the dust temperature towards the nucleus, in this case, is a result of the increasing attenuation of the solar radiation as it penetrates the dust halo.

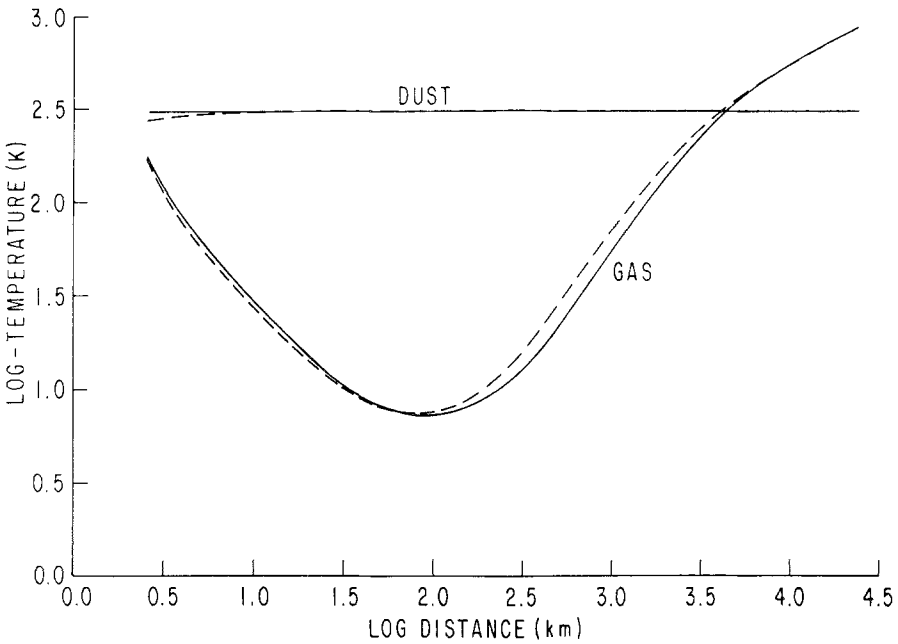

Fig. 4. Radial profiles of the temperature of gas and dust in the supersonic region. Solid lines correspond to the PMS-model while the broken lines correspond to the DE-model.

The variations of the dust and gas temperatures in the supersonic region are shown in Figure 4. While the dust temperature remains more or less constant the gas temperature first falls to a minimum of about 6 K around 60 km from the nucleus before increasing to about 700 K at $r \approx 10^4$ km. This gas temperature profile is almost identical to that obtained in Paper I, where dust was ignored. Although it has been suggested that the hot dust in the inner coma could be a significant source of heating for the gas (Shulman, 1969), our calculations do not seem to bear this out. In fact we deliberately chose a highly absorbing material for the dust, in order to make the temperature difference between the dust and gas in the inner coma sufficiently large. Even so the transfer of heat from the dust to the gas does not seem to have been sufficient to offset the rapid cooling due to expansion and IR emission by H_2O. Of course, we have used a fixed grain size ($a = 1\mu$). Since the total effective area of all the grains of a fixed size for a given mass of dust varies inversely as their size, selection of $a = 0.3\mu$, would have increased the effective total area, and therefore the heat transfer rate from the dust to the gas by over a factor of 3. Even so, we do not expect the gas temperature profile in the inner coma to be changed significantly, because of the predominance of the IR-cooling. As is seen from Equation (20), the

LTE IR-cooling rate in the inner coma $\propto n_{H_2O} \propto r^{-2}$, whereas the heating rate by the dust $\propto n_{H_2O} n_d \propto r^{-4}$. Consequently, except in a region very close to the nucleus, the heating by the dust will be overwhelmed by the IR-cooling.

The profiles of the Mach number and the gas and dust velocity profiles in the supersonic region are shown in Figure 5. In both models the Mach number increases to a maximum of about 10 around the point at which the temperature reaches a minimum. Thereafter it decreases due to the efficiency of photolytic heating in the outer coma reaching a value of about 2.5 at $r \approx 10^4$ km. While the gas velocity increases to about 1.5 km s^{-1} in the outer coma, the dust reaches a terminal speed of around 0.25 km s^{-1}, and 0.20 km s^{-1} in the PMD-model and the DE-model, respectively.

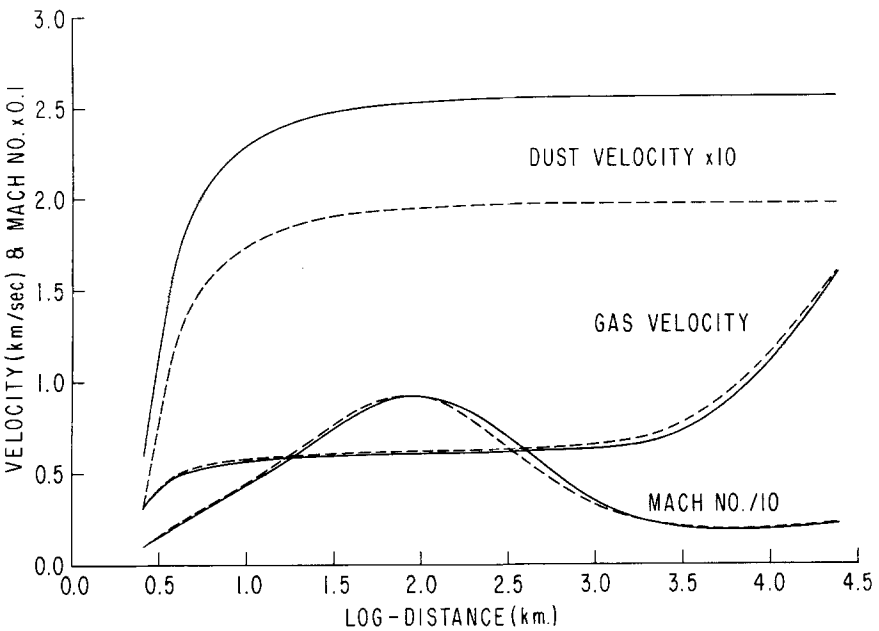

Fig. 5. Radial profiles of the Mach number, the gas velocity and the dust velocity in the supersonic region. Solid lines correspond to the PMD-model, while the broken lines correspond to the DE-model.

The number density profiles of the dominant neutral species are shown in Figure 6, while those of the ionic species are shown in Figure 7. Just as in the case of the dust-free atmosphere of Paper I, the maximum ion density in the inner coma is about a factor 5 less than those predicted by earlier models. The reason for this, as we pointed out in Paper I, is two-fold. Firstly, the dissociative recombination processes, which removes electrons in the inner coma, is seen from Table I to be highly temperature dependent, being more efficient at lower temperatures. If extrapolation of these rate coefficients down to temperatures as low at 5 K is permissible (see Paper I), they would increase by over a factor of 3 when T changes from 100 to 10 K. This could partly be responsible

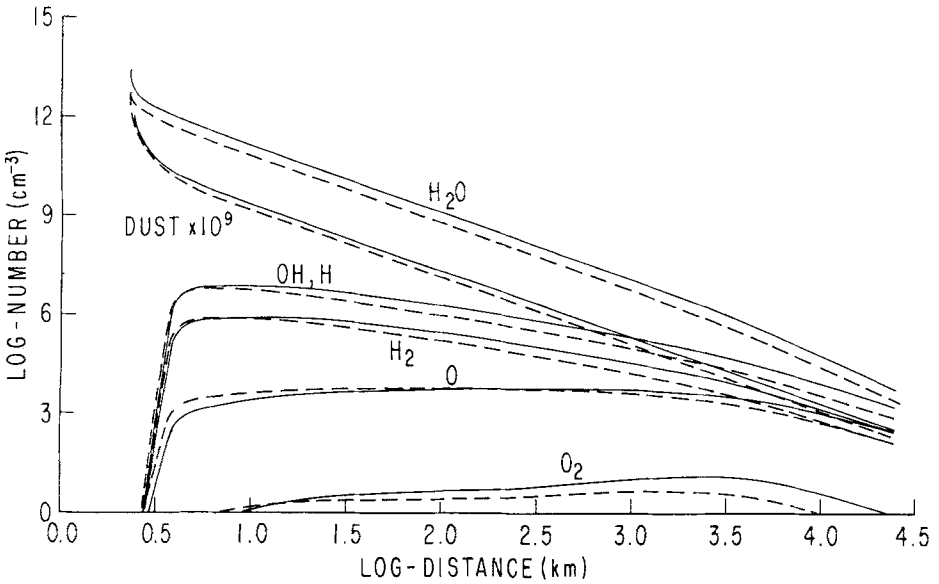

Fig. 6. Radial profiles of the number densities of the neutral gas species and the dust within the entire collision-dominated coma. Solid lines correspond to the PMS-model, while the broken lines correspond to the DE-model.

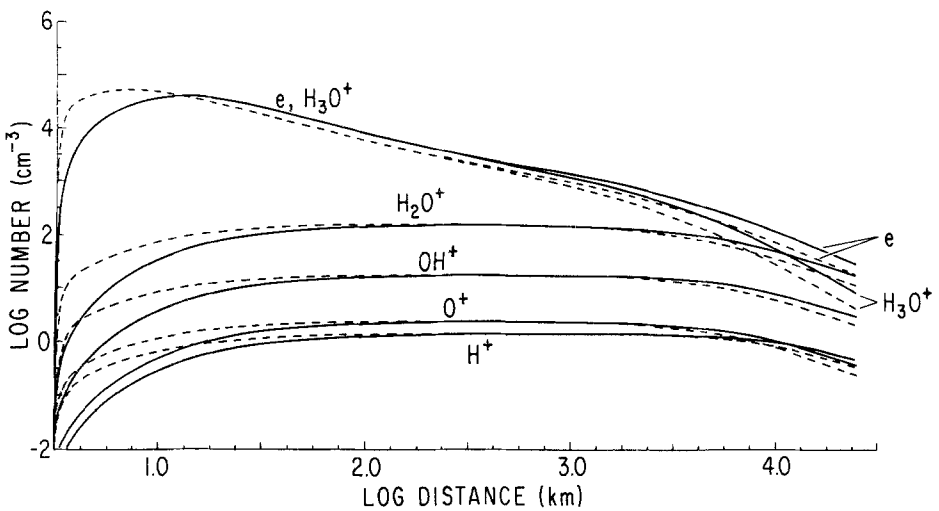

Fig. 7. Radial profiles of the number densities of the ions and electrons within the entire collision-dominated coma. Solid lines correspond to the PMS-model, while the broken lines correspond to the DE-model.

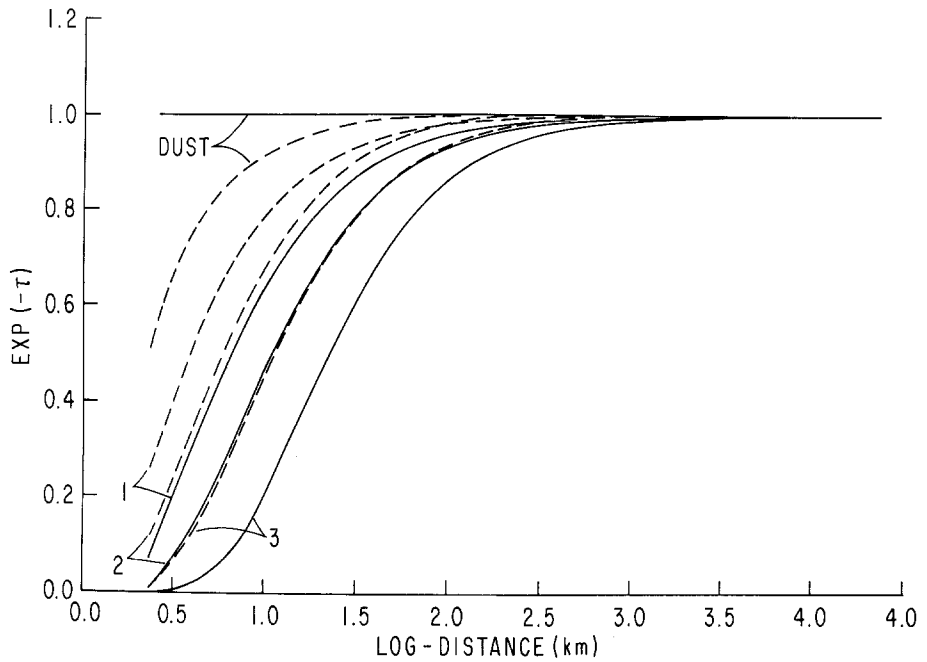

Fig. 8. The attenuation of the UV fluxes J_1, J_2, J_3 and the total solar radiant energy flux I. The curves marked (1), (2), (3) and dust are, respectively, $J_1(r)/J_1(\infty)$, $J_2(r)/J_2(\infty)$, $J_3(r)/J_3(\infty)$ and $I(r)/I(\infty)$. The solid lines correspond to the PMS-model, while the broken lines correspond to the DE-model.

for the depletion of the electron density in the inner coma. Also, the UV radiation flux that is responsible for the photo-ionization of H_2O is J_3, and this is the one that suffers the strongest attenuation in the inner coma (see Figure 8). If, instead of considering the attenuation of the three bands separately, we had taken into account only the attenuation of the total solar UV radiation $(J_1+J_2+J_3)$ in the calculation of the photo-ionization rates, as is usually the practice, we would have overestimated the electron density in the inner coma, because J_1, in which about 90% of the solar UV flux is contained, is also the least strongly attenuated (see Figure 1). Also (from Figure 7), the electron density in the inner coma in the PMS-model is seen to be significantly smaller than in the DE-model, while the opposite is the case in the outer coma. The reason for this is that the production rate of the electrons is approximately proportional to the product of number density of H_2O and the extinction $(e^{-\tau})$ of J_3. Consequently, in the outer coma where the extinction is negligible, the production rate of electrons would be greater in the PMS-model (see Figure 6). On the other hand, near the nucleus, the extinction of J_3 in the PMS-model is larger, due to the larger column densities of H_2O and dust, and this more than offsets the larger H_2O density there. Consequently, the production rate of electrons is now smaller than in the DE-model.

All the above results correspond to the case when the dust to gas production ratio, $\chi = 1$. It is interesting to investigate the effects of varying χ on the flow, particularly in the subsonic region. Two other values of χ, namely $\chi = 0.5$, corresponding to a relatively dust-free comet, and $\chi = 2$, corresponding to a very 'dusty' comet, have been used for the purpose. We have confined ourselves to the PMS-model. The variation of the Mach number at the nuclear surface, M_S, and the thickness of the subsonic region, Δ, are exhibited in Table II. Clearly M_S decreases, as expected, and Δ increases correspondingly, as χ increases. A similar trend is expected in the DE-model also.

TABLE II

Variation of M_S and Δ with χ (PMS-model)

χ	M_S	Δ (m)
0.5	0.82	26
1	0.69	85
2	0.52	274

In conclusion we note that the neglect of possible 'parent' molecules other than H_2O is a limitation of our model. The addition of even more species considerably complicates the atmospheric chemistry. However, as we have stated earlier, as long as H_2O is the predominant parent molecule, the change will be mainly in the chemical structure of the atmosphere and not in its temperature and velocity profiles, which have been the main concern of this paper. While the temperature profile will be predominantly controlled by the H_2O molecule, the dust will play an important role, in determining the velocity profile, particularly in the inner coma. A more accurate treatment of this problem, in the future, will have to take into account multiple scattering by the dust more explicitly, perhaps following a scheme similar to that of Weissman and Kieffer (1981). But the most important improvement that is required, is the relaxation of the 1-fluid treatment of the gas. The gas velocity and temperature profiles that have been calculated may reasonably be expected to represent those of the heavier species, although even here the temperature may be an overestimate beyond $r \approx 10^3$ km (Ip, 1982). On the other hand, they are likely to bear little resemblance to those of the lightest neutral species, H, which initially carries off much of the excess energy during the dissociation of H_2O, as well as OH. Interpretation of Ly-α isophotes and line profiles seem to indicate rapid outflow of hydrogen in the outer coma. In fact, the existence of two separate H-components, one with a mean outflow velocity of 8 km s^{-1} (believed to arise from the photo-dissociation of OH) and one with a mean outflow velocity of 20 km s^{-1} (believed to arise from the photo-dissociation of H_2O) have been proposed (e.g., Keller, 1973; Meier *et al.*, 1976). What is therefore required is a multifluid approach to the problem. While all the heavier species may be lumped together to form a single fluid, the H has to be treated separately. Such a study is presently in progress (Marconi and Mendis, 1982b).

Acknowledgments

We acknowledge support from the following grants: NASA-NGR-05-009-110 of the NASA Planetary Atmospheres program; NASA-NSG-7102 of the NASA Geophysics and Geochemistry program; NASA-NSG-7623 of the NASA Space Plasma program and NSF-AST-81-08706 of the NSF Astronomy program.

References

Allen, C. W.: 1976, *Astrophysical Quantities*, Athlone Press, p. 172.
Hanner, M. S.: 1980, *Solid Particles in the Solar System*, I. Halliday and B. A. McIntosh (eds.), D. Reidel Publ. Co., Holland, p. 223.
Hellmich, R.: 1979, Ph.D. thesis, University of Göttingen, W. Germany.
Hellmich, R.: 1981, *Astron. Astrophys.* **93,** 341.
Houpis, H. L. F. and Mendis, D. A.: 1981, *Astrophys. J.* **243,** 1088.
Huebner, W. F.: 1981, private communication.
Huffman, D. R.: 1982, private communication.
Ip, W-H.: 1982, unpublished preprint ('On the photochemical heating of cometary comas: The cases of H_2O and CO-rich comets').
JANAF Thermo-Chemical Tables, Second Edition, 1971 (National Bureau of Standards).
Keller, H. U.: 1973, *Astron. Astrophys.* **23,** 269.
Marconi, M. L. and Mendis, D. A.: 1982a, *Astrophys. J.* (in press). Paper I.
Marconi, M. L. and Mendis, D. A.: 1982b, (in preparation).
Meier, R. R., Opal, C. B., Keller, H. U., Page, T. L. and Carruthers, G. R.: 1976, *Astron. Astrophys.* **52,** 283.
Probstein, R. F.: 1968, *Problems of Hydrodynamics and Continuum Mechanics*, M. Lavrent'ev (ed.), Philadelphia: SIAM, p. 568.
Sekanina, Z. and Miller, F. D.: 1973, *Science* **179,** 565.
Shimizu, M.: 1975, *The Study of Comets*, NASA-SP 393, B. Donn, M. Mumma, W. Jackson, M. A'Hearn and R. Harrington (eds.), p. 763.
Shimizu, M.: 1976, *Astrophys. Space Sci.* **40,** 149.
Shul'man, L. M.: 1981, *Astrometriya i Astrofizika* **4,** 101, Kiev (NASA TT F-599).
van de Hulst, H.C.: 1981, *Light Scattering by Small Particles*, Dover, New York.
Weissman, P. R. and Kieffer, H. H.: 1981, *Icarus* **47,** 302.
Whipple, F. L.: 1950, *Astrophys. J.* **111,** 375.
Zucrow, M. J. and Hoffmann, J. D.: 1976, *Gas Dynamics*, Vol. 1, John Wiley, N.Y., p. 56.